Water Resources Research

RESEARCH ARTICLE
10.1029/2019WR025571

Flood Size Increases Nonlinearly Across the Western United States in Response to Lower Snow-Precipitation Ratios

Frances V. Davenport[1], Julio E. Herrera-Estrada[1,2,3], Marshall Burke[1,4,5], and Noah S. Diffenbaugh[1,6]

[1]Department of Earth System Science, Stanford University, Stanford, CA, USA, [2]Program on Water in the West, Stanford University, Stanford, CA, USA, [3]Descartes Labs, New York, NY, [4]Center on Food Security and the Environment, Stanford University, Stanford, CA, USA, [5]National Bureau of Economic Research, Cambridge, MA, USA, [6]Woods Institute for the Environment, Stanford University, Stanford, CA, USA

Key Points:
- Stream gages show an approximately exponential increase in streamflow peak size in response to lower snow fraction of runoff
- Rainfall-driven floods can be more than 2.5 times as large as snowmelt-driven floods, so a shift toward more rain can increase flood risk
- Snow-dominated and mixed-regime watersheds could see larger floods under warmer winter conditions if precipitation amounts remain similar

Supporting Information:
- Supporting Information S1

Correspondence to:
F. V. Davenport,
fvdav@stanford.edu

Citation:
Davenport, F. V., Herrera-Estrada, J. E., Burke, M., & Diffenbaugh, N. S. (2020). Flood size increases nonlinearly across the western United States in response to lower snow-precipitation ratios. *Water Resources Research*, *56*, e2019WR025571. https://doi.org/10.1029/2019WR025571

Received 15 MAY 2019
Accepted 18 DEC 2019
Accepted article online 20 DEC 2019

Abstract Many mountainous and high-latitude regions have experienced more precipitation as rain rather than snow due to warmer winter temperatures. Further decreases in the annual snow fraction are projected under continued global warming, with potential impacts on flood risk. Here, we quantify the size of streamflow peaks in response to both seasonal and event-specific rain-fraction using stream gage observations from watersheds across the western United States. Across the study watersheds, the largest rainfall-driven streamflow peaks are >2.5 times the size of the largest snowmelt-driven peaks. Using a panel regression analysis of individual precipitation and snowmelt events, we show that the empirical streamflow response grows approximately exponentially as the liquid precipitation input increases, with rain-dominated runoff leading to proportionately larger streamflow increases than snowmelt or mixed rain-and-snow runoff. We find that the response to changes in rain percentage is largest in the wettest watersheds, where wet antecedent conditions are important for increasing runoff efficiency. Similarly, the effect of rain percentage is larger across watersheds in the Northwest and West regions compared to watersheds in the Northern Rockies and Southwest regions. Overall, as a higher percentage of precipitation falls as rain, increases in the size of rainfall-driven and "rain-on-snow"-driven floods have the potential to more than offset decreases in the size of snowmelt-driven floods.

1. Introduction

Seasonal snowpack acts as an important natural reservoir, reducing the likelihood of winter floods and providing water in the spring and summer when demand exceeds supply from precipitation (Barnett et al., 2005; Gleick, 1987). Recently, warmer temperatures have decreased both the percentage of winter precipitation falling as snow and annual snowpack accumulation (Das et al., 2009; Feng & Hu, 2007; Knowles et al., 2006a; Mote, 2006; Mote et al., 2018). Likewise, large decreases in snow fraction and snow accumulation are projected to occur in response to continued global warming (Ashfaq et al., 2013; Gleick, 1987; Stewart, 2009). Decreases in snow fraction are associated with a higher elevation of freezing and an overall decrease in the area where snow occurs (Klos et al., 2014). A shift from snow to rain thus carries potential consequences for water resources (Berghuijs et al., 2014) and flood risk (Huang et al., 2018).

Rainfall and snowmelt are both important mechanisms for flood generation in mountainous or snow-dominated regions (Berghuijs et al., 2016; Parajka et al., 2010; Pitlick, 1994). As a result, accounting for both snowmelt and precipitation intensity is essential for accurately predicting flood size (Harpold & Kohler, 2017; Yan et al., 2018). There is evidence that warmer conditions have already initiated a shift towards more rain-dominated flood regimes (Huang et al., 2018), with snowmelt occurring earlier in the year (Blöschl et al., 2017; Dettinger et al., 2004; Hall et al., 2014; Hamlet et al., 2006; Stewart et al., 2005), and many watersheds seeing an increased number of annual peak floods caused by rainfall (Fritze et al., 2011; Kampf & Lefsky, 2016). Rain-on-snow events, which are associated with some of the largest floods in snow-dominated regions (Harr, 1981; Kattelmann, 1997; Sui & Koehler, 2001), are becoming more frequent at high elevations and less frequent at low elevations, with this pattern expected to continue in the future (Freudiger et al., 2014; McCabe et al., 2007; Musselman et al., 2018).

However, because both the baseline temperature and the rate of warming will influence the transition from snow to rain under different levels of future warming, the likelihood of snow becoming rain in the future may not be uniform across all geographic areas or parts of the precipitation distribution. For example, both the mean temperature and rate of warming of atmospheric rivers, which deliver cold-season moisture to the western United States (US), have been shown to vary by latitude (Gonzales et al., 2019). Likewise, in the Sierra Nevada and Cascades, intense precipitation has historically been warmer than less-intense precipitation (suggesting that wet extremes could have greater potential to transition to liquid precipitation) but may also be warming at a slower rate (Rupp & Li, 2017).

Despite evidence of transitions toward more rain-dominated flooding, previous studies have generally found a lack of significant trends in flood magnitude (Archfield et al., 2016; Hodgkins et al., 2017; Lins & Slack, 1999; Slater & Villarini, 2016). Similarly, there have been very few significant trends in runoff efficiency at the annual scale (McCabe et al., 2018), despite robust decreases in annual snow fraction and evidence that lower snow fractions can lead to reduced runoff efficiency (Berghuijs et al., 2014). The lack of significant trends highlights difficulties in understanding impacts of warming on streamflow, in part because a long time series (>100 years) is often necessary to detect robust changes in streamflow (Wilby, 2006; Ziegler et al., 2005). However, in terms of changes in flood risk, some patterns may be emerging. In colder, high-elevation watersheds, declining trends in annual peak flows are more common than increasing trends (Rood et al., 2016; Solander et al., 2017; Vormoor et al., 2016). Historical warming has likely increased flood magnitude for mixed-regime watersheds (Hamlet & Lettenmaier, 2007), with similar increases in flood risk projected in the future (Das et al., 2011; Loukas et al., 2002; Tohver et al., 2014). Overall, the existing literature suggests some heterogeneity in the watershed-scale response to global warming, with changes in flood magnitude not yet detectable for most watersheds.

A shift from snow to rain could affect the size of floods through a number of mechanisms. For example, lower snowmelt intensity is projected under warmer conditions (Musselman et al., 2017), which could lead to smaller snowmelt-driven floods. Alternatively, higher rain percentages mean more liquid water available for runoff immediately following precipitation (assuming similar amounts of precipitation). With a higher elevation of freezing, there is a larger contributing area for runoff production and the potential for much larger flood events from rain (Kattelmann, 1997; Tohver et al., 2014). Whether rainfall-driven floods could become larger than historical snowmelt-driven floods also depends on whether future rain rates could exceed historical snowmelt rates. Recent climate modeling evidence suggests that warming-induced decreases in snow-to-rain ratio lead to increased flood risk (Huang et al., 2018; Li et al., 2019). However, the magnitude of the watershed flood response to variations in rain/snow fraction has not been quantified using a generalized empirical framework.

In this study, we use 410 gaged watersheds across the western US to explore the role of snowfall in moderating flood size. It is well known that the western US is heavily dependent on snowfall for water availability, with over 50% of streamflow estimated to come from snow each year (Li et al., 2017). Recent events, such as the 2017 flood season that caused over $1 billion in infrastructure damage in California, also highlight the significance of winter flooding in this region (Tavares & Kracher, 2017). However, there is high uncertainty around the specifics of future flood risk, because traditional approaches to estimate risk are no longer appropriate under nonstationary climate conditions (CSIWG, 2018; Milly et al., 2008). Predictions of future flood risk will benefit from improved understanding of flooding processes and of how these processes respond to warming (Merz & Blöschl, 2003).

We investigate the relationship between snow and flood risk using two approaches: (a) by analyzing the streamflow conditions that immediately follow precipitation and snowmelt and (b) by analyzing the precipitation and snowmelt conditions that immediately precede the largest streamflow peaks. Together, these analyses quantify how the snow fraction of precipitation modifies the size of streamflow peaks both immediately following precipitation and later in the season.

To conduct these analyses, we construct datasets of historical precipitation events, historical snowmelt events, and historical streamflow peaks in each watershed. We use a panel regression analysis to quantify the response of streamflow in each watershed to individual precipitation and snowmelt events. This analysis relies on historical variations in the rain percentage of runoff within each watershed to understand how rain percentage impacts subsequent streamflow response.

Exploiting within-unit variation over time is a common econometric approach for identifying causal relationships in observational data and is increasingly used in hydrologic studies (Bassiouni et al., 2016; Steinschneider et al., 2013). Panel regression builds on a number of traditional approaches to offer valuable new insights. For example, relative to standard cross-sectional regression, the panel regression allows us to isolate the role of snow fraction from other time-invariant factors that could also be associated with flood size (e.g., warmer, wetter regions could have larger floods on average). Using within-unit variation also offers advantages over trend detection (which is a common alternative approach to quantifying the streamflow response to climate-driven changes), as robust trend detection requires a long time series, and the effect of climate-driven changes on streamflow can be hard to distinguish from other long-term changes.

We complement the panel analysis with a summary analysis of the precipitation and snowmelt conditions preceding the largest streamflow peaks in each watershed. To identify the mechanisms responsible for the largest events in each watershed, we categorize each streamflow peak as primarily snowmelt-driven, rainfall-driven or "rain-on-snow"-driven. We then compare the distribution of streamflow peaks, snowmelt intensity, and precipitation intensity as a function of average seasonal snow fraction. These analyses, combined with the panel regression, provide a new understanding of the sensitivity of streamflow peaks to the fraction of precipitation falling as snow or rain.

2. Methods

2.1. Watershed Selection

We use daily-mean streamflow observations from US Geological Survey (USGS) stream gages. We focus our study on the conterminous United States west of 105°W. We identify stream gages using the Geospatial Attributes of Gages for Evaluating Streamflow (GAGES-II) dataset (Falcone et al., 2010). We use the dataRetrieval package in the R computing language to download daily streamflow data for each gage (Hirsch & De Cicco, 2015). In total, we include streamflow data from a total of 410 watersheds (see Figure 1a for a map of the locations of the stream gages included).

We include stream gages that (a) have at least 20 years of daily streamflow observations during water years 1980 through 2016 (where each year has fewer than 10% of days with missing data); (b) report data during all months; and (c) do not have periods of zero flow lasting one month or more. We use 20 years of data as a minimum requirement to capture a representative climatology at each location (requiring all 37 years of data would reduce the number of available sites by 40%). To exclude gages where streamflow is likely to be influenced by upstream reservoir operations, we remove stream gages with upstream storage exceeding 1,000 acre-feet (1,233,000 m^3; around 50% of gaged watersheds in the region are below this threshold, and watersheds with upstream reservoirs are likely to have storage capacity on the order of thousands or millions of acre-feet; Martin & Hanson, 1966) We include two gages on the same river if the downstream gage has a contributing watershed area at least twice that of the upstream gage. If the two watersheds are closer in size, we only include the larger watershed. We include watersheds that have experienced at least one rainfall-driven, one rain-on-snow-driven, and one snowmelt-driven streamflow peak (see section 2.6 for a description of streamflow peak identification).

2.2. Precipitation and Land Surface Data

We use output from the Variable Infiltration Capacity (VIC) model from Phase 2 of the North American Land Data Assimilation System (NLDAS-2) to characterize climatological and event-specific precipitation and snow variables for each watershed. NLDAS-2 covers the entire study area with 1/8° spatial resolution and hourly temporal resolution (Xia et al., 2012). From VIC, we use hourly rainfall, snowfall, snow water equivalent (SWE), and total column soil moisture. The precipitation forcing for NLDAS-2 is derived from a gage-only Climate Prediction Center analysis, with an orthographic adjustment based on the PRISM climatology. Other forcing fields for NLDAS-2 (including temperature) are derived from the NCEP North American Regional Reanalysis.

In order to capture subgrid-scale topographic complexity, VIC uses "elevation-banding" within the snow module (Mitchell et al., 2004; Sheffield et al., 2003). Hourly temperature is adjusted within each elevation band based on a temperature lapse rate. Precipitation phase partitioning within each band is based on a temperature threshold. For temperatures above 0 °C, all precipitation is rain. At or below 0 °C, all precipitation is

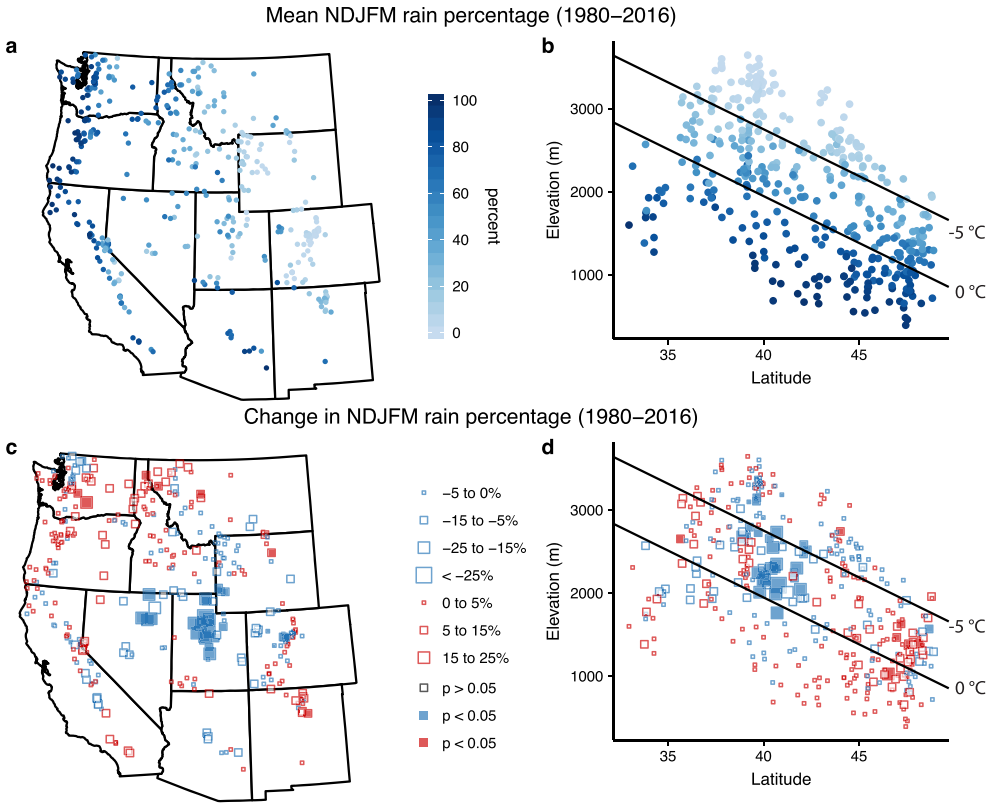

Figure 1. (a) Locations of the 410 US Geological Survey (USGS) stream gage stations used in the analysis, with color corresponding to mean watershed November through March (NDJFM) rain percentage over the 1980–2016 time period. (b) Mean NDJFM rain percentage plotted by elevation and latitude for the same stations as in (a). The sloping lines represent the 0 °C and −5 °C isotherms. Isotherms are calculated using a multiple linear regression of NDJFM temperature on elevation and latitude, following the method described in Mote (2006). (c) Absolute change in NDJFM rain percentage over the 37-year time period estimated based on the nonparametric Theil-Sen slope for each watershed. Red (blue) squares indicate increasing (decreasing) trends. Filled squares show trends that are significant (p value <0.05) using a Mann-Kendall trend test. (d) Change in NDJFM rain percentage plotted by elevation and latitude. Sloping lines are the same isotherms shown in (b).

snow. Water and energy budgets for the snow module are solved independently for each elevation band. VIC also includes subgrid vegetation tiles within each elevation band. For all variables, we calculate watershed average values by taking an area-weighted average of all grid cells that overlap with the watershed boundary (as defined in the GAGES-II dataset).

For our summary analysis, we characterize the influence of rain-versus-snow in each watershed using the percentage of cold-season precipitation that falls as rain during each water year. To maintain consistency with previous studies (Feng & Hu, 2007; Knowles et al., 2006a; Mankin & Diffenbaugh, 2015), we define the cold-season as November through March ("NDJFM"). We calculate the mean NDJFM rain percentage for each watershed as the average of the annual NDJFM values during the 1980–2016 time period.

To compare historical precipitation and snowmelt intensity, we calculate 1-day, 3-day, and 8-day precipitation and snowmelt rates over water years 1980–2016 in each watershed, using hourly precipitation and snowmelt output from VIC. We calculate the maximum precipitation intensity and maximum snowmelt intensity in each watershed for each of the three timeframes (1-day, 3-day, and 8-day). We then calculate the ratio of the maximum precipitation intensity to maximum snowmelt intensity in each watershed to determine their relative magnitudes.

2.3. Streamflow Event Analysis

We identify and compare the largest rainfall-driven, snowmelt-driven, and rain-on-snow-driven streamflow events in each watershed to characterize the relative importance of rainfall and snowmelt in generating the

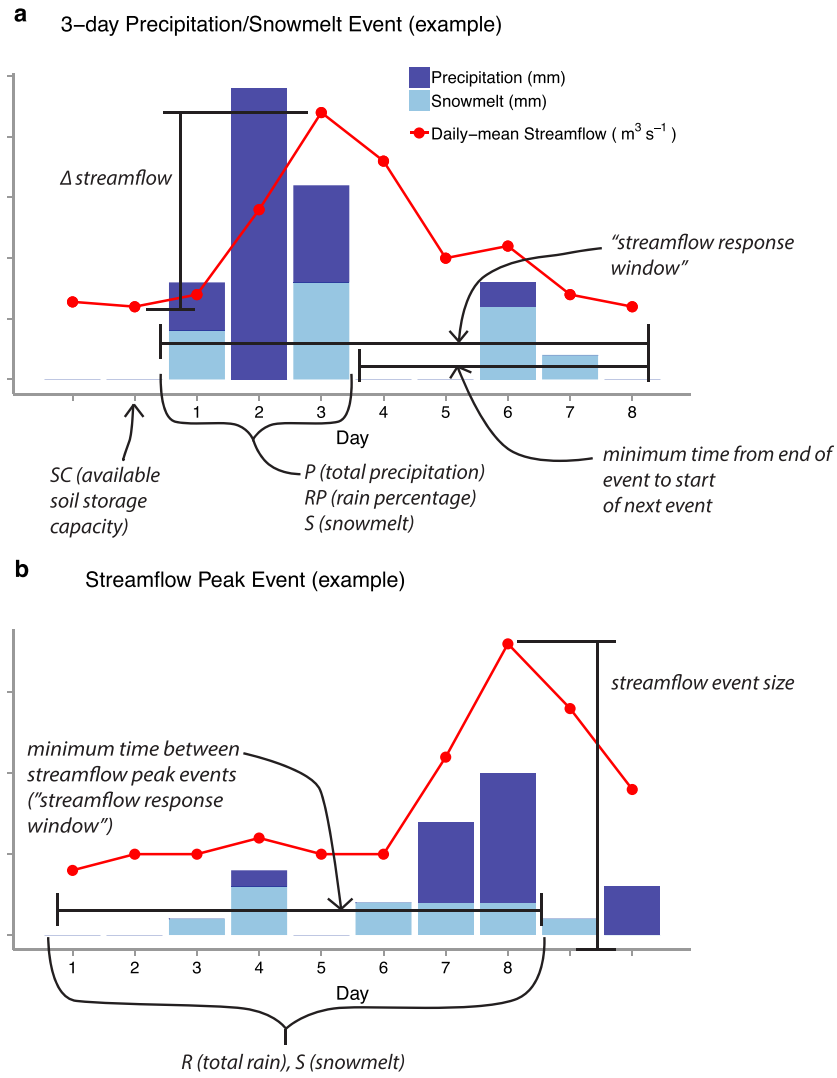

Figure 2. (a) Schematic of 3-day precipitation and/or snowmelt events used in the panel regression analysis. Daily precipitation totals are shown in dark blue, daily snowmelt totals are shown in light blue, and the daily-mean streamflow time series is shown in red. Total precipitation (P), rain percentage (RP), and snowmelt (S) are calculated over the 3-day precipitation event. The increase in streamflow (Δ streamflow) is calculated as the increase in streamflow within the 8-day "streamflow response window." Available subsurface storage capacity (SC) is calculated as the average available storage capacity in the watershed before the start of the 3-day precipitation event. (b) Schematic of streamflow event identification. Daily precipitation totals are shown in dark blue, daily snowmelt totals are shown in light blue, and the daily-mean streamflow time series is shown in red. Total rain (R) and snowmelt (S) are calculated as the sum of all rain and snowmelt over the 8-day "streamflow response window."

largest historical streamflow events. We identify streamflow events from the 1980–2016 gage observations using a peaks-over-threshold approach. At each gage, we use the median daily-mean streamflow value as the exceedance threshold and calculate all historical peaks that exceed this value. To capture precipitation and snowmelt leading up to each streamflow event, we define an 8-day response window for each event, but in this case, the window begins 7 days before the streamflow peak and ends on the day of the streamflow peak (see Figure 2b). To avoid events with overlapping windows, we only include peaks separated by at least seven days. Peaks that are separated by fewer than 7 days are considered part of one event, and only the largest of those peaks is included in the analysis.

From the VIC output, we calculate the total rain, total snow, and net change in SWE over the 8-day window leading up to the observed streamflow event. Snowmelt during the 8-day window is calculated as the net decrease in SWE over the period and is defined as zero if the net change in SWE is zero or positive. (Here,

snowmelt refers to melting of the existing snowpack, so snowmelt is zero if SWE is zero at the start of the 8-day period).

In order to better understand the differences between rainfall-driven and snowmelt-driven streamflow events, we classify streamflow events into three flood types (snowmelt-driven, rainfall-driven, and rain-on-snow-driven) based on the total rain and total snowmelt over the 8-day window. Previous studies of rain-on-snow events have used a range of thresholds to define rain-on-snow, including any amount of rain and a decrease in SWE (Surfleet & Tullos, 2013), 1 mm/day of rain and a decrease in SWE (Jeong & Sushama, 2017), and 10 mm/day of rain on top of snowpack with at least 10 mm SWE (Musselman et al., 2017). We use an intermediate threshold of 10 mm of rain and/or snowmelt over the 8-day window. For this study, rainfall-driven events include events where the total rain exceeds 10 mm leading up to the event, but snowmelt is less than 5 mm. Snowmelt-driven events are those where snowmelt exceeds 10 mm, but total rain is less than 5 mm. Rain-on-snow-driven events occur when both total rain and snowmelt exceed 5 mm. (Note that not all streamflow events fall into these three categories.)

We identify the largest streamflow event of each type within each watershed. (We divide streamflow by drainage area and mean annual watershed precipitation to normalize across watersheds.) We then test differences in magnitude between the three flood types using a paired Wilcoxon signed-rank test. We adjust p values using the Bonferroni method to account for the fact that multiple tests are conducted using the same sample (Wright, 1992). We also group the watersheds into five equally spaced categories based on mean NDJFM rain percentage (i.e., 0–20% rain, 20–40% rain, ... , 80–100% rain), and test differences between the flood types within each watershed group. These comparisons allow us to understand how the distributions of the largest floods differ between snow-dominated, mixed-regime, and rain-dominated watersheds.

2.4. Precipitation and Snowmelt Event Identification

To complement the analysis of historical streamflow peaks (section 2.3), we also analyze the streamflow response following individual precipitation and snowmelt events. We first calculate 3-day precipitation totals in each watershed using hourly precipitation from the NLDAS-2 precipitation forcing (Figure 2a; we define precipitation as zero on days where the 24-hr total is less than 1 mm). We calculate 3-day snowmelt totals as the net decrease in SWE over each 3-day period using SWE from the VIC model output (snowmelt is defined as 0 if a positive change in SWE occurs). We define individual precipitation/snowmelt runoff events based on combined 3-day totals of precipitation and snowmelt (if precipitation or snowmelt occurs over more than or fewer than three consecutive days, we define the event as the period with the maximum 3-day total). Events can be due to only precipitation, only snowmelt, or a combination of precipitation and snowmelt. Events must be separated by at least 5 days (Ivancic & Shaw, 2015) between the end of one event and the start of the next event; otherwise, only the event with the greater 3-day maximum is included. The number of precipitation events in each watershed ranges from 350 to 903, due to differences in precipitation patterns and in the length of record at each stream gage.

For each event, we record (a) the rain percentage of the water available for runoff (total rain divided by the combined total of precipitation and snowmelt), (b) total 3-day precipitation, (c) net 3-day snowmelt, and (d) the available subsurface storage in the watershed. Snowmelt-only events are included as 0% rain events. Events with rain percentages between 0 and 100 have a combination of rain, snow, and/or snowmelt at different times during the 3-day period or in different parts of the watershed. Available subsurface storage is calculated as the total soil storage capacity minus total column soil moisture before the precipitation event (using the VIC soil moisture and storage capacity fields).

Watersheds across the US typically show a lag of 5 days or less between rainfall and streamflow response (Ivancic & Shaw, 2015). We therefore define a streamflow response window as the 8-day period beginning on the first day of the 3-day precipitation event and ending 5 days after the event (see Figure 2a for a schematic diagram; the minimum separation of 5 days between precipitation events ensures that two events are not associated with the same runoff response). We calculate the streamflow response (Δ *streamflow*) following each precipitation event as the maximum streamflow within the streamflow response window minus the streamflow before precipitation started (i.e., the increase in streamflow within the response window). If there is no increase in streamflow following the precipitation event, we assign an arbitrary streamflow

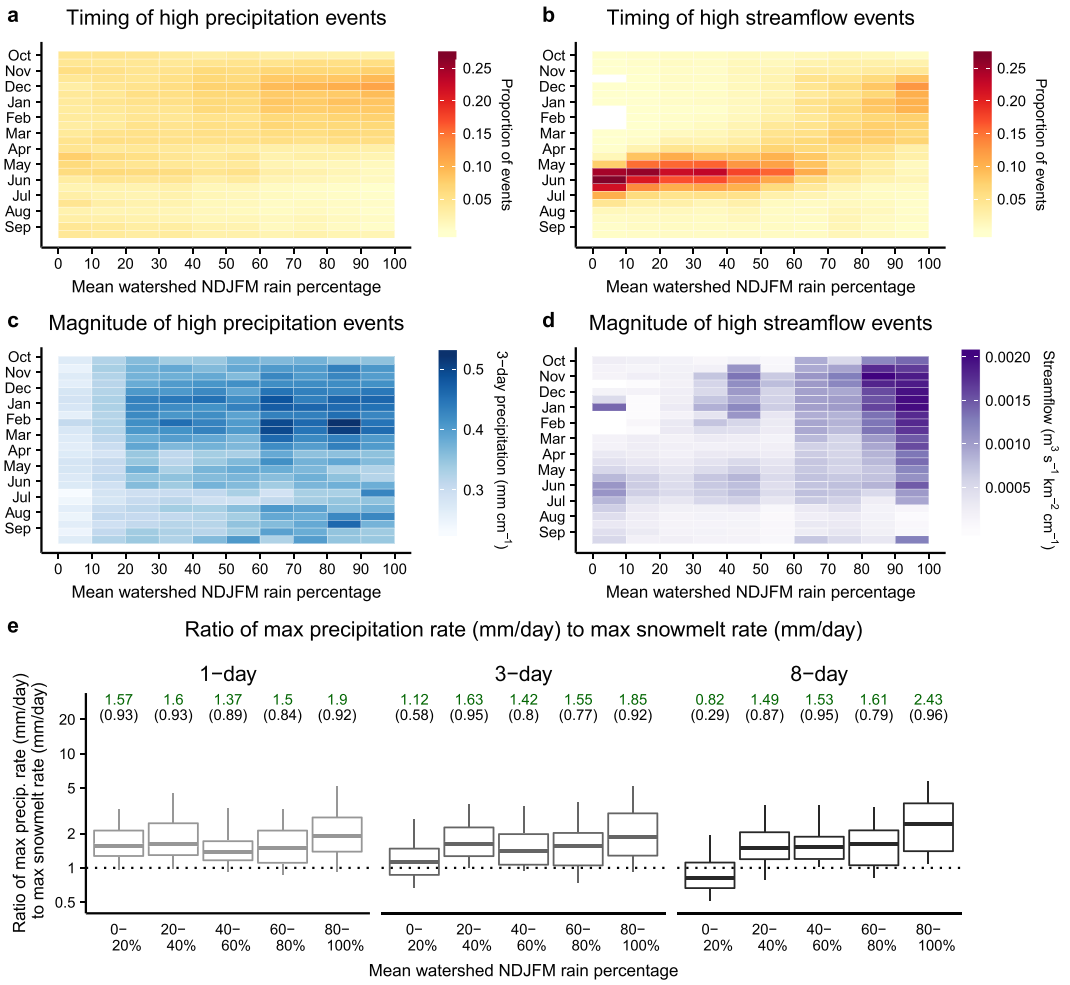

Figure 3. (a) Timing of the largest quartile of precipitation events in each watershed by mean watershed November through March (NDJFM) rain percentage. Frequency is calculated as the proportion of events within each column that occur during each time of year. (b) Same as (a) but for the largest quartile of streamflow events in each watershed. (c) Magnitude of the largest quartile of precipitation events in each watershed, by time of year and mean watershed NDJFM rain percentage. Three-day precipitation event magnitudes (mm) are divided by mean annual watershed precipitation (cm). Magnitude for each row-column combination is calculated as the median of all events with that combination. (d) Same as (c) but for the largest quartile of streamflow events in each watershed. Streamflow event magnitudes ($m^3\ s^{-1}$) are divided by watershed drainage area (km^2) and mean annual watershed precipitation (cm). (e) Ratio of maximum precipitation rate (mm/day) to maximum snowmelt rate (mm/day) in each watershed. Precipitation rates and snowmelt rates are averaged over the entire watershed for 1-day, 3-day, and 8-day periods. The center line of each box shows the median event for that group of watersheds, the bottom and top boundaries of the box represent the 25th and 75th percentiles, respectively, and the whiskers extend to the 5th and 95th percentiles, respectively. The median ratio for each group is shown in green (numbers in parentheses indicate the proportion of watersheds with a ratio > 1).

increase of 0.01 $ft^3\ s^{-1}$ (0.00028 $m^3\ s^{-1}$) to enable the log transformation used in the panel regression model (see below).

2.5. Panel Regression Model

The analysis of historical streamflow events (described in section 2.3) uses a "space-for-time" substitution to show how the largest streamflow events vary by average watershed rain percentage. However, across the study watersheds, average NDJFM rain percentage is moderately correlated with average annual precipitation ($r = 0.54$) and slightly correlated with slope ($r = 0.36$; supporting information Figure S1a–b). Therefore, for the analysis of precipitation/snowmelt events, we use a panel regression model that allows us to control for both static and time-varying factors that affect streamflow and could be correlated with rain percentage.

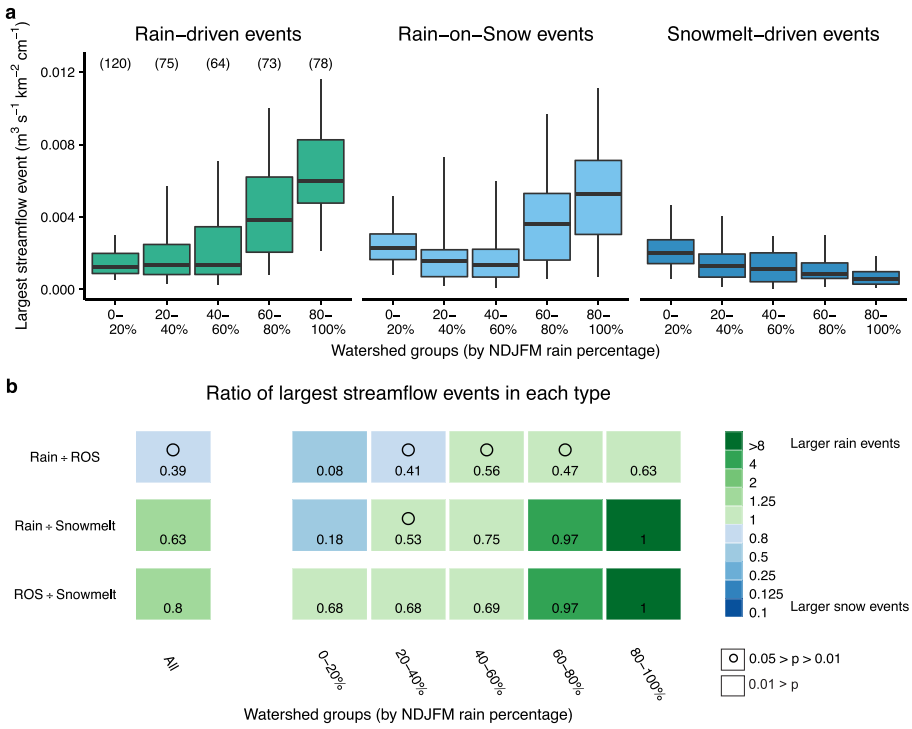

Figure 4. (a) Distribution of the maximum rainfall-driven, rain-on-snow-driven, and snowmelt-driven flow events in each watershed by mean watershed November through March (NDJFM) rain percentage. Streamflow events are standardized by dividing by watershed drainage area (km^2) and mean annual watershed precipitation (cm). The center line of each box shows the median event for that group, the bottom and top boundaries of the box represent the 25th and 75th percentiles, respectively, and the whiskers extend to the 5th and 95th percentiles, respectively. The number of watersheds in each group are shown in parentheses. (b) Ratio of largest streamflow events of each type by watershed NDJFM rain percentage and across all watersheds. Ratios are calculated using the median event from each distribution. Blue (green) boxes indicate that events with snow (rain) are larger. The symbol in each box represents the adjusted p value from the paired Wilcoxon signed-rank sum test; boxes without symbols have p values less than 0.01. The number in each box indicates the proportion of watersheds with a ratio > 1.

Using a multi-dimensional panel dataset that includes observations across time and space can enable more robust estimates of hydrologic response compared to traditional time-series analysis or cross-sectional ("space-for-time") regressions (Steinschneider et al., 2013). When pooling across watersheds, it is necessary to account for differences in the average streamflow response between watersheds resulting from factors such as drainage area, average climate, and land use. We include watershed-specific fixed effects, μ_i, to account for these time-invariant, average differences in the streamflow response between watersheds. Further, we include month fixed effects specific to each watershed to account for seasonal differences (such as rates of insolation or evapotranspiration) that could confound the relationship between rain percentage and streamflow. Additionally, there is the possibility of temporal trends in each watershed due to unrelated factors (i.e., changes in the streamflow response over time due to human activity such as land cover change). To account for this possibility, we include a linear time trend in each watershed. In essence, the regression models the streamflow response to each precipitation or snowmelt event compared to other events within the same watershed, after controlling for the calendar month and year. For more detail on panel regression methodology, see Steinschneider et al. (2013), who provide a thorough discussion on the application of panel regressions to hydrologic studies.

In the regression, we also include the total precipitation (P), available subsurface storage capacity (SC), and snowmelt (S) as independent variables for each event. The general form of the regression equation used is as follows:

$$\log(y_{i,k}) = f(RP_{i,k}) + \beta_1 P_{i,k} + \beta_2 SC_{i,k} + \beta_3 S_{i,k} + \mu_i + \gamma_{im} + \theta_i t + \varepsilon_{i,k,}$$

where $y_{i,k}$ is the streamflow response (Δ *streamflow*) following the kth precipitation event in watershed i; $f(RP_{i,k})$ models the effect of rain percentage; β_1 through β_3 are regression coefficients for precipitation (P), subsurface storage capacity (SC) , and snowmelt (S), respectively; μ_i represents the fixed effect for watershed i; γ_{im} are a set of watershed-month fixed effects; θ_i is the linear time trend for watershed i; and $\varepsilon_{i,k}$ is an error term. We include three specifications for $f(RP_{i,k})$: a log-linear function, a piecewise function, and a step function. The latter two specifications allow for a more flexible response between rain percentage and log(Δ *streamflow*).

For the piecewise model, we create five truncated rain percentage variables (RP_{j}) that each capture the effect of rain percentage over an interval of 10 percentage points (Schlenker & Roberts, 2009; Toms & Lesperance, 2003). For example, RP_1 models the effect on streamflow as rain percentage increases from 0% to 20%, RP_2 models the effect on streamflow as rain percentage increases from 20% to 40%, ... , and RP_5 models the effect on streamflow as rain percentage increases from 80% to 100%. Within each of these intervals, the regression assumes a linear relationship between rain percentage and log(Δ *streamflow*). A given rain percentage is mapped to these variables such that the new variable has a value of 20 if rain percentage is above that interval, a value of 0 if rain percentage is below that interval, and a value equal to the rain percentage minus the lower bound if the rain percentage is within that interval. For example, if the event rain percentage is 32%, RP_1 is assigned a value of 20, and RP_2 is assigned a value of 12. This approach ensures continuity at the interval break points.

To model $f(RP_{i,k})$ as a step function, we create binary variables to group events by rain percentage within intervals of 10 percentage points. For example, one variable is used to indicate events that are between 0 and 10% rain, a second variable indicates events that are between 10 and 20% rain, and so on. We use smaller bins of 10 percentage points for the step function to allow for a more flexible response function (Schlenker & Roberts, 2009). The first variable (indicating events with 0–10% rain) is used as the "reference" group and is not included in the regression. The coefficients estimated for the remaining variables describe events in each group relative to events in the reference group.

We use the lfe package in the R computing language to compute the panel regression coefficients (Gaure, 2013).

2.6. Quantifying Robustness of the Panel Regression

We use a bootstrap resampling technique (Efron & Tibshirani, 1986) to quantify uncertainty in the estimated regression coefficients. For each bootstrap iteration, we randomly sample with replacement from the original set of 410 stream gages to obtain a new set of 410 stream gages, where some gages are included multiple times, and others are not included at all. We recalculate the panel regression coefficients for the new dataset using all three model specifications. We repeat this process 1,000 times and use the distribution of estimated coefficients to measure uncertainty in the response functions. For each bootstrap replicate, we also calculate the difference between the piecewise model slopes and the slope for the simple log-linear specification. This results in a distribution of differences for each interval, which we use to test the difference between the piecewise model and the log-linear model.

Each response function characterizes the average response across all watersheds. Due to the large range of climates and physical characteristics represented by the watersheds in our study, we also test the sensitivity of the modeled response function to a number of watershed characteristics. We group watersheds into the driest third, the wettest third, and the middle third, based on mean annual precipitation. We also group watersheds by size into the smallest, middle third, and largest thirds, and by slope into the flattest, middle, and steepest thirds. We test the sensitivity of the response among watersheds with low and high degrees of human alteration (using the "reference" and "nonreference" designations in GAGES-II to define low and high alteration, respectively). Lastly, we group the watersheds into the four National Center for Environmental Information (NCEI) climate regions that cover the western US (Northwest, West, Southwest, and Northern Rockies). We repeat the same bootstrapping procedure to estimate uncertainty around the response function within each subset of watersheds.

3. Results

3.1. Hydroclimatic Characteristics of Western US Watersheds Based on Mean Rain Percentage

The 410 watersheds experience a wide range of winter conditions, with some watersheds receiving almost entirely rain and some watersheds receiving almost entirely snow (Figure 1a). As expected, most watersheds with low rain percentages are located at high elevations or high latitudes (Figure 1b). Likewise, watersheds with high rain percentages are mostly located at lower elevations. Watersheds with winter temperatures between the 0 °C and −5 °C elevation-latitude isotherms receive a mix of rain and snow over the cold season. Most watersheds have not experienced significant changes in cold-season rain percentage over the 1980–2016 period ($p > 0.05$; Figure 1c). The watersheds that have experienced significant trends ($p < 0.05$) are mostly located between the 0 °C and −5 °C elevation-latitude isotherms (Figure 1d). In these watersheds, both increasing and decreasing trends have occurred. These changes in the rain percentage of precipitation could result from changes in temperature, shifts in the timing of precipitation (towards either warmer or colder parts of the season), or both.

Figure 3 shows the seasonal patterns of the largest (top 25%) precipitation and streamflow events as a function of mean watershed NDJFM rain percentage. The timing of precipitation events is similar across watersheds, with more frequent precipitation in November through March and less frequent precipitation in June through August (Figure 3a). Average watershed rain percentage is correlated with average annual precipitation (Figure S1). Because spring snowmelt is a critical component of streamflow in colder watersheds, the timing of high streamflow is very dependent on the average watershed NDJFM rain percentage (Figure 3b). In watersheds with less than 50% rain, streamflow peaks tend to be concentrated later in the season, with a majority (70%) of events occurring May through July. In contrast, in watersheds with high rain percentages, most high streamflow events occur at the same time of year as large precipitation events (Figure 3b).

The magnitude of the largest streamflow events (Figure 3d) is not a direct reflection of the size of precipitation events (Figure 3c). The largest streamflow events occur in warmer watersheds with >80% NDJFM rain, although the size of precipitation events is fairly consistent across watersheds with >40% NDJFM rain (Figure 3c). Additionally, the coldest watersheds (<10% rain) have larger streamflow peaks than watersheds with 10–40% rain (Figure 3d), despite having smaller precipitation events (Figure 3c).

Our analysis of streamflow events (Figure 4) supports earlier conclusions that both rain and snowmelt are important sources of runoff during peak streamflow, although the size of snowmelt-driven vs. rainfall-driven streamflow peaks varies depending on the average watershed rain percentage (to control for differences in precipitation between watersheds, we standardize streamflow by dividing by mean annual precipitation and watershed area). Snowmelt-driven events are largest in the coldest watersheds (0–20% rain), whereas rainfall-driven events and rain-on-snow events are largest in the warmest watersheds (80–100% rain; Figure 4a). Interestingly, the smallest rain-on-snow events occur in watersheds with 40–60% rain. While rain-on-snow events often lead to the largest streamflow peaks, 39% of watersheds have rainfall-driven streamflow peaks that are larger than rain-on-snow-driven peaks, and 20% of watersheds have snowmelt-driven peaks that are larger than rain-on-snow-driven peaks (Figure 4b). In watersheds with >80% rain, 63% of watersheds have rainfall-driven streamflow peaks that are larger than rain-on-snow streamflow peaks (Figure 4b).

Overall, these results suggest a nonlinear increase in the size of rainfall-driven and rain-on-snow-driven streamflow peaks as the average watershed rain percentage increases (Figure 4a). Rainfall-driven streamflow peaks in the warmest watersheds (>80% rain) are more than 4.5 times as large as rainfall-driven streamflow peaks in the coldest watersheds (0–20% rain). This is not surprising because most of the precipitation in the coldest watersheds falls as snow, meaning a significant portion of runoff is delayed until spring snowmelt. However, rainfall-driven streamflow peaks in the warmest watersheds (>80% rain) are still more than 2.5 times as large as snowmelt-driven streamflow peaks in the coldest watersheds (0–20% rain).

We compare snowmelt intensity with precipitation intensity in each watershed to evaluate whether historical snowmelt rates exceed historical precipitation rates (Figure 3e). For the majority of watersheds, maximum precipitation rates exceed maximum snowmelt rates over 1-day and 3-day timescales. In the coldest watersheds (0–20% rain), precipitation rates exceed snowmelt rates for 93% of watersheds within the 1-

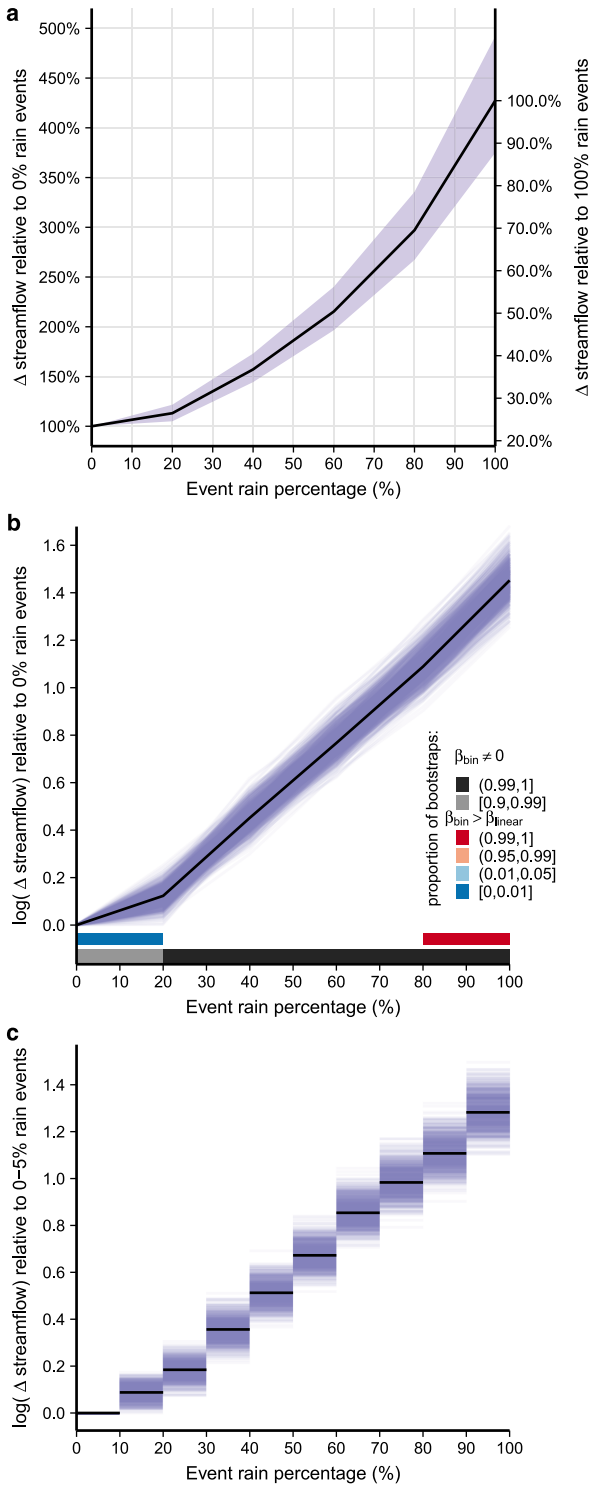

Figure 5. (a) Historical response of streamflow to changes in event rain percentage. Results from the piecewise regression using log(Δ streamflow) as the dependent variable are transformed to show percentage changes in Δ streamflow (black line). The left (right) axis shows Δ streamflow relative to 0% (100%) rain events. Purple shading indicates the 95% confidence interval from bootstrapping the results 1,000 times. Bootstrap samples were generated by randomly selecting stream gage stations with replacement from the stations shown in Figure 1. (b) As in (a), but with y-axis showing log(Δ streamflow) response. Purple lines show the individual response functions estimated from each bootstrap iteration. Gray colors along the x-axis indicate the proportion of bootstrap replicates that estimated statistically significant effects of rain percentage within each bin. Red/blue colors along the x-axis indicate the proportion of bootstrap replicates where the estimated bin slope was larger than the slope of a simple log-linear model calculated across the entire range of rain percentages. (c) Results of the regression using a step function specification. Purple lines show individual bootstrap estimates, using the same bootstrapping procedure as in (a) and (b).

Table 1
Selected Coefficients From Piecewise Linear Regression (see Methods section 2.5)

	Dependent variable: log(Δ streamflow)
Subsurface storage capacity (mm)	−0.001*** (0.0001)
Precipitation (mm)	0.037*** (0.0002)
Snowmelt (mm)	0.092*** (0.001)

Note. Standard error for each coefficient shown in parentheses.
*$p < 0.1$. **$p < 0.05$. ***$p < 0.01$

day timeframe, for 58% of watersheds within the 3-day timeframe, and for 29% of watersheds within the 8-day timeframe (Figure 3e). Among watersheds with >20% rain, a majority have precipitation rates that exceed snowmelt rates at all three timescales.

3.2. Effect of Rain Fraction on the Response of Streamflow to Precipitation/Snowmelt Events

We use the panel regression to measure the effect of increasing rain percentage on the streamflow response immediately following precipitation and snowmelt events. As expected, the shift from snow-dominated precipitation and snowmelt to rain-dominated precipitation significantly affects streamflow, with higher rain percentages leading to a larger streamflow response (Figure 5). As suggested by our analysis of streamflow peaks (Figure 4), the effect of increasing rain percentage is nonlinear. For example, for a given precipitation amount, events with 100% rain contain twice as much liquid precipitation as events with 50% rain, but generate streamflow increases that are approximately 2.4 times as large (Figure 5a). Similarly, precipitation events that are 100% rain have 25% more liquid precipitation than events that are 80% rain, but generate streamflow increases that are, on average, 33% larger. We find that the streamflow response estimated between 0 and 20% is consistently flatter than the slope estimated for the log-linear model, meaning the effect of increasing rain percentage is lower in this range (Figure 5b). At rain percentages above 20%, the piecewise model is not significantly different from the log-linear model. Thus, the effect of increasing rain percentage on the streamflow response is approximately exponential in this range.

The step function shows a similar effect of rain percentage on streamflow response (Figure 4c); that is, there is a smaller change in the response of streamflow to increases in rain percentage below 20% and an approximately log-linear relationship above 20%. We find that precipitation amount and concurrent snowmelt also have statistically significant ($p < 0.01$) positive effects on the streamflow response, although the effect of snowmelt is larger than that of precipitation (Table 1). As expected, antecedent subsurface storage capacity has a significant ($p < 0.01$) negative effect on the streamflow response, meaning that more available soil storage reduces the streamflow response (Table 1).

The magnitude of the estimated response function is sensitive to average watershed precipitation amount, with the wettest watersheds exhibiting the strongest response to changes in rain percentage (Figure 6a). Consistent with this result, the response to increased rain percentage is larger in the Northwest region (Oregon, Washington, and Idaho) compared to other regions, although the differences between geographic regions are less pronounced than the differences between precipitation regimes (Figure 6e). The response function is less sensitive to physical watershed characteristics like slope and drainage (Figures 6b and 6c). The mean response is largest for the steepest watersheds, but the uncertainty bounds overlap for the three groups (Figure 6b). The steepest watersheds are also some of the wettest (Figure S1), so the larger mean response may result from the correlation between average precipitation and watershed slope. In agreement with recent work showing that natural and managed watersheds respond similarly to climatic changes (Ficklin et al., 2018), we find similar response functions between watersheds with varying degrees of human alteration (Figure 6d). Taken together, these sensitivity tests identify some important differences in the streamflow response across watersheds, although the pattern of nonlinear increases in response to increasing rain percentage is robust. Overall, the sensitivity testing shown in Figure 6 suggests that the fixed effects in the regression model control well for static watershed characteristics like slope, area, and degree of alteration.

4. Discussion

We have quantified changes in the streamflow response to variations in the fraction of precipitation and runoff from snow and rain. Overall, snow-dominated watersheds have smaller flood peaks than mixed-regime or rain-dominated watersheds (Figures 3 and 4a). In addition, in the panel regression analysis of streamflow immediately following individual precipitation and snowmelt events, we find that the empirical relationship between rain percentage and the subsequent streamflow response is nonlinear, with rain-dominated runoff leading to proportionately larger streamflow peaks than snowmelt-dominated or mixed rain-and-snow runoff (Figures 5 and 6). However, changes in rain percentage have a smaller effect when rain percentage is below 20%.

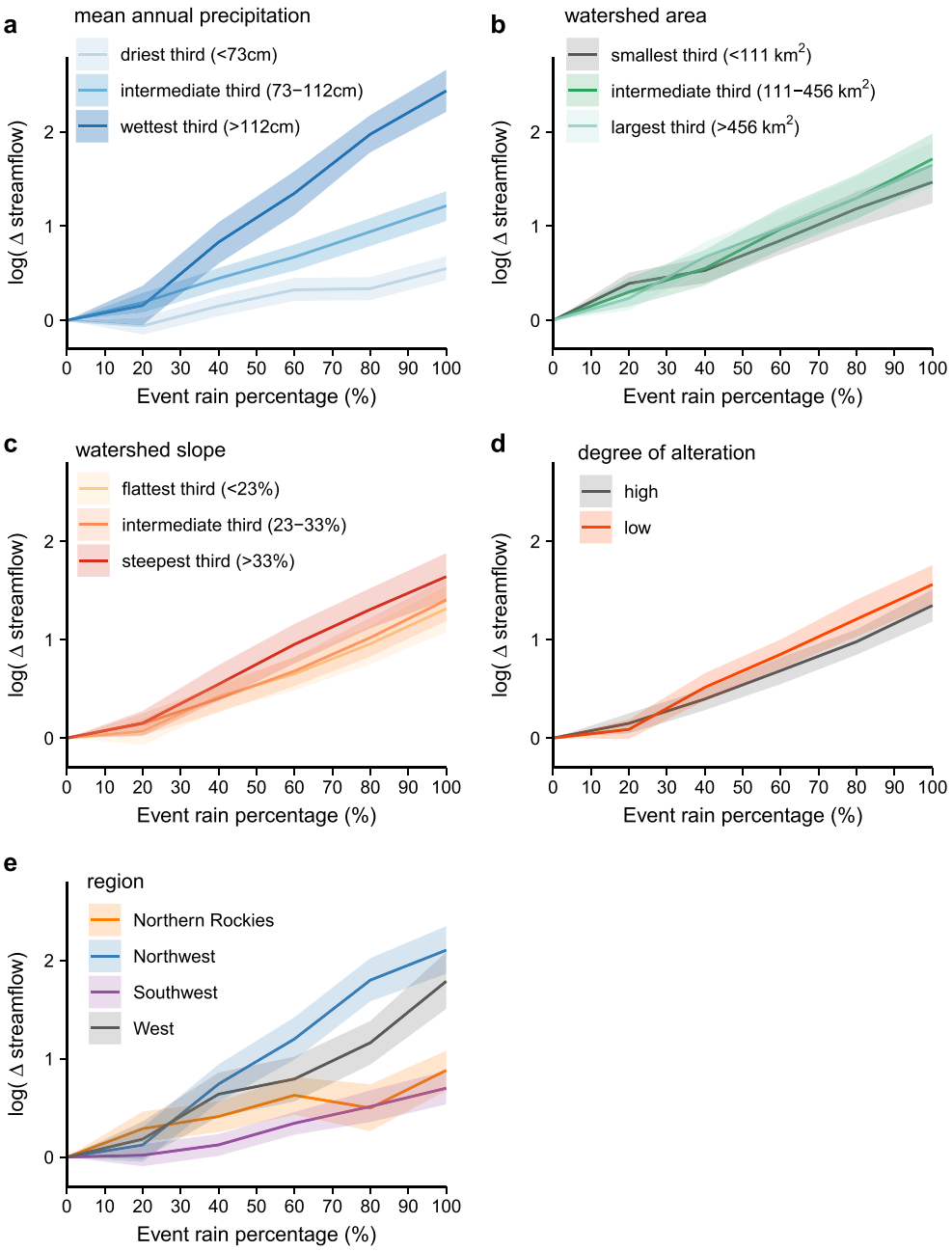

Figure 6. Panel regression results for subsets of the study watersheds. (a) Watersheds grouped into the driest third (<73 cm mean annual precipitation), intermediate third (73–112 cm mean annual precipitation), and wettest third (>112 cm mean annual precipitation). (b) Watersheds grouped into the smallest third (<111 km^2), intermediate third (111–456 km^2), and largest third (>456 km^2). (c) Watersheds grouped by flattest third (<23% slope), intermediate third (23–33% slope), and steepest third (>33% slope). (d) Watersheds grouped by degree of human alteration based on the "reference" (low alteration) and "nonreference" (higher alteration) designations from the Geospatial Attributes of Gages for Evaluating Streamflow (GAGES-II) database. (e) Watersheds grouped by National Center for Environmental Information (NCEI) climate regions. In all panels, shading shows the 95% bootstraped confidence intervals for each group.

Compared to previous work that analyzed snowmelt and precipitation intensity at snow telemetry sites (Fassnacht & Records, 2015; Harpold & Kohler, 2017; Yan et al., 2018, 2019), our results indicate a smaller proportion of sites where snowmelt intensity exceeds precipitation intensity, especially on short (1-day or 3-day) timescales. Yan et al. (2019) also found that annual maximum snowmelt rates have been decreasing throughout the region, while annual maximum precipitation rates have shown no change or have increased slightly. The difference between previous studies and the snowmelt vs. precipitation rates presented in our

study could result from biases in modeled snowmelt compared to snow telemetry observations but may also reflect the difference between snowmelt rates at the scale of a monitoring station versus at the scale of an entire watershed. Whereas precipitation can cover an entire watershed, snowmelt is unlikely to occur at all elevations within a watershed at once. Our comparisons of snowmelt rates with precipitation intensity at the watershed scale suggest that, as a larger percentage of precipitation falls as rain, it is possible that runoff rates during rainfall events could exceed maximum historical snowmelt rates for most watersheds.

Nonlinearity in streamflow peaks has been observed in multiple studies (Robinson et al., 1995; Sivapalan et al., 2002) and can arise from a number of factors including the amount of liquid water input, antecedent conditions that impact runoff efficiency (Vivoni et al., 2007), and physical watershed characteristics (Vivoni et al., 2008). Event rain percentage, the independent variable in our panel regression, is a measure of the liquid water input during each event, and, thus, liquid water input is likely the primary driver of the nonlinear response estimated in the regression. Differences in precipitation intensity during rain compared with mixed rain-and-snow precipitation could also contribute to the nonlinear response. Higher streamflow-to-snowmelt ratios have also been found during faster snowmelt conditions (Barnhart et al., 2016), which may be more likely to occur during warmer, mixed rain-and-snowmelt events.

The sensitivity analysis (Figure 6) reveals that streamflow in the wettest watersheds is more sensitive to changes in rain percentage than streamflow in the driest watersheds. This difference highlights the importance of wet antecedent conditions in watersheds receiving the most precipitation and suggests more efficient partitioning of rain into streamflow in wetter watersheds. While physical watershed characteristics such as average slope and watershed area have important effects on differences in streamflow across watersheds, these characteristics do not significantly affect the within-watershed response to changes in rain percentage (Figure 6). In other words, the steepest and flattest watersheds experience a similar percent change in streamflow following an increase or decrease in rain percentage. However, watershed topography could contribute to the modeled response function shown in Figures 5 and 6, as the distribution of elevation (hypsometry) located below the freezing level changes for each precipitation or snowmelt event. Thus, runoff efficiency could increase as larger or steeper portions of each watershed are exposed to above-freezing conditions (i.e., as rain percentage increases).

Our analysis of streamflow events (Figure 4a) agrees with previous work showing that snowmelt-driven peaks decrease in size as the seasonal rain fraction increases (Harpold & Kohler, 2017; Rood et al., 2016; Solander et al., 2017). At the same time, the panel regression (Figures 5 and 6) shows that increases in rain fraction lead to larger streamflow peaks. Thus, if the timing and amount of precipitation in the western US remains similar in the future but rain fraction increases as projected (e.g., Ashfaq et al., 2013), increases in rainfall-driven and rain-on-snow-driven streamflow peaks could be larger than decreases in snowmelt-driven streamflow peaks, especially given that maximum precipitation rates exceed maximum snowmelt rates for the majority of watersheds (Figure 3).

However, the change in rain percentage needed for rainfall-driven streamflow peaks to exceed snowmelt-driven streamflow peaks will likely vary across watersheds. In mixed-regime watersheds (>50% NDJFM rain), rainfall-driven and rain-on-snow-driven streamflow peaks are similar or slightly larger than the largest snowmelt-driven peaks (Figure 4b). Therefore, higher rain percentages could immediately lead to increases in the largest streamflow peaks. In colder watersheds (typically at high latitude and/or high elevation), historical snowmelt-driven peaks are larger than rainfall-driven peaks, and larger reductions in snow-to-rain ratios may be required before the magnitudes of rainfall-driven peaks exceed those of historical snowmelt-driven floods. Temporary reductions in flood risk due to decreases in the size of snowmelt-driven floods are also possible for the coldest watersheds, especially if warming causes some snowmelt to occur earlier in the season, reducing the amount of water stored in snowpack in the spring.

These patterns are consistent with earlier work reporting that snow-dominated watersheds are more likely to experience decreasing or insignificant trends in flood size, whereas warmer mixed-regime watersheds are more likely to have experienced increasing trends in flood size (Hamlet & Lettenmaier, 2007; Loukas et al., 2002). Similarly, Li et al. (2019) found that a majority of watersheds along the west coast experience increases in the 100-year flood risk as the amount of snow decreases under future warming, but that changes in 100-year flood risk are likely to be more varied for watersheds in the Rocky Mountains. Building on these earlier studies, our results provide additional insight into how the size of floods varies between watersheds with

different snow regimes and why increasing rain percentages can have a more immediate impact on high streamflow in mixed-regime watersheds than in the coldest watersheds. Further, our results show that the wettest watersheds (particularly those in the Northwest and West regions) show the highest sensitivity to changes in rain percentage.

We note a number of considerations for evaluating our results. One source of uncertainty is the relatively coarse (1/8°) resolution of NLDAS-2 compared to the topographic complexity of mountainous watersheds. To evaluate this uncertainty, we compare the NLDAS topography to a 30 m digital elevation model (Figure S2). The NLDAS-2 elevation grid gives unbiased estimates of mean watershed elevation but overestimates low elevations and underestimates high elevations within each watershed. NLDAS-2 represents the hypsometric curve of large watersheds more accurately than for small watersheds. Because the VIC model uses elevation banding to model subgrid-scale topographic complexity, these comparisons represent the upper bound on disagreement, as the subgrid elevation banding provides additional heterogeneity within each grid point. Further, we note that although the coarse model grid could affect the modeled snowfall and snowmelt used in our analyses, all of our streamflow calculations rely on stream gage observations and therefore reflect the true watershed hypsometry.

There is also uncertainty associated with modeled estimates of snow and rain partitioning, as well as SWE. For example, recent work suggests that precipitation phase partitioning is not well captured by a simple temperature threshold model (Harpold et al., 2017). To assess the error associated with modeled SWE, we compare VIC SWE estimates with 766 SNOTEL monitoring sites (Figure S3a–b). VIC SWE estimates show strong correlation with SNOTEL observations (60% of locations have correlations above 0.75) but frequently have a negative bias (Figure S3b). The differences between VIC and SNOTEL are likely due to a combination of model error and scale mismatch between the point observations and the NLDAS-2 grid. Given the scale mismatch, we also compare SWE calculated from VIC with that calculated from the higher resolution Sierra Nevada Snow Reanalysis ("SNSR"; Margulis et al., 2016) for the 53 watersheds that overlap with the SNSR domain (Figure S3c–d). At the watershed scale, VIC SWE estimates are highly correlated with SNSR, including 57% of watersheds with correlations above 0.90. Additionally, the VIC SWE values exhibit smaller bias relative to SNSR than relative to SNOTEL. While snow pillow observations may provide the most accurate estimates of SWE, the existing monitoring stations only measure SWE at point locations that are mostly situated at lower and middle elevations, making them poor estimators of watershed-scale SWE (Bales et al., 2006; Painter et al., 2016). Previous research indicates that simulated SWE estimates covering a larger spatial extent can predict streamflow as well or better than point observations (Rosenberg et al., 2011). Likewise, assessments of NLDAS-2 found that the VIC model captures the seasonal streamflow cycle very well in mountainous regions, indicating that the modeled snowmelt estimates are appropriate for the basin-wide analyses used in this study (Cai et al., 2014; Xia et al., 2012).

Finally, there are limitations with the streamflow observations. We use daily-mean streamflow observations, which are available over a longer time period and for more stations than instantaneous streamflow estimates. However, daily-mean streamflow can underestimate the magnitude of instantaneous streamflow peaks, particularly for events with the fastest response times. Snowmelt-driven streamflow often has a diurnal signal due to a peak in snowmelt rates in the afternoon (Lundquist et al., 2005). Therefore, our results may underestimate the streamflow response to rain events where the peak duration is much shorter than 1 day or for snowmelt-driven events where streamflow is likely to rise and fall throughout the day. Our analysis also excludes stream gages that only operate seasonally because of freezing conditions at the gage site. As a result, the coldest watersheds may be slightly underrepresented in our analysis, although our results still include watersheds that receive almost exclusively snow precipitation over the November–March period (Figure 1).

5. Conclusions

Our results reveal an approximately exponential response of streamflow to rain/snow fraction over the western United States during the 1980–2016 period. That relationship implies large potential for continued regional warming to increase flood risk, even without changes in precipitation frequency, magnitude, or timing. Rain causes significantly larger flood events than snow, both within watersheds and across our watershed sample. The approximately exponential relationship means that decreasing snow fraction leads

to proportionally larger increases in streamflow. Further, the wettest watersheds show the largest response to changes in rain/snow fraction. Extrapolating from our empirical results, wet, mixed-regime watersheds, such as those along the coastal ranges, can be expected to see the most immediate increases in flood size in response to continued warming. In contrast, high-elevation snow-dominated watersheds may see more delayed changes in flood risk, due to the competing influence of decreasing snowmelt-driven floods and increasing rainfall-driven floods.

Increases in flood risk pose a particularly difficult challenge for the western US, where infrastructure is already vulnerable to winter flooding events (CSIWG, 2018). Our results provide a new, comprehensive quantification of the contribution of snowfall to flood control in the region. The approximately exponential relationship identified in our results emphasizes that temperature-induced changes in snow fraction are likely to strongly influence future changes in flood risk, regardless of uncertainty about future changes in total precipitation.

Data Availability Statement

The daily stream gage data are available from the United States Geological Survey (https://waterdata.usgs.gov/nwis/sw). The GAGES-II dataset is available from https://doi.org/10.3133/70046617. The NLDAS-2 Forcing data (https://doi.org/10.5067/6J5LHHOHZHN4) and VIC model output (https://doi.org/10.5067/ELBDAPAKNGJ9) are available from the NASA Goddard Earth Sciences Data and Information Services Center. Source code for the analysis is available at https://github.com/fdavenport/WRR2019.

Acknowledgments
We thank three anonymous reviewers and the editors for insightful and constructive comments. We thank the USGS for access to the stream gage data and NASA for providing access to the NLDAS-2 data. Computational resources were provided by CEES and SRCC at Stanford University. Funding was provided by Stanford University.

References

Archfield, S. A., Hirsch, R. M., Viglione, A., & Blöschl, G. (2016). Fragmented patterns of flood change across the United States. *Geophysical Research Letters*, *43*, 10,232–10,239. https://doi.org/10.1002/2016GL070590

Ashfaq, M., Ghosh, S., Kao, S.-C., Bowling, L. C., Mote, P., Touma, D., et al. (2013). Near-term acceleration of hydroclimatic change in the western U.S. *Journal of Geophysical Research: Atmospheres*, *118*, 10,676–10,693. https://doi.org/10.1002/jgrd.50816

Bales, R. C., Molotch, N. P., Painter, T. H., Dettinger, M. D., Rice, R., & Dozier, J. (2006). Mountain hydrology of the western United States. *Water Resources Research*, *42*, W08432. https://doi.org/10.1029/2005WR004387

Barnett, T. P., Adam, J. C., & Lettenmaier, D. P. (2005). Potential impacts of a warming climate on water availability in snow-dominated regions. *Nature*, *438*(7066), 303–309. https://doi.org/10.1038/nature04141

Barnhart, T. B., Molotch, N. P., Livneh, B., Harpold, A. A., Knowles, J. F., & Schneider, D. (2016). Snowmelt rate dictates streamflow. *Geophysical Research Letters*, *43*, 8006–8016. https://doi.org/10.1002/2016GL069690

Bassiouni, M., Vogel, R. M., & Archfield, S. A. (2016). Panel regressions to estimate low-flow response to rainfall variability in ungaged basins. *Water Resources Research*, *52*, 9470–9494. https://doi.org/10.1002/2014WR016618

Berghuijs, W. R., Woods, R. A., & Hrachowitz, M. (2014). A precipitation shift from snow towards rain leads to a decrease in streamflow. *Nature Climate Change*, *4*(7), 583–586. https://doi.org/10.1038/nclimate2246

Berghuijs, W. R., Woods, R. A., Hutton, C. J., & Sivapalan, M. (2016). Dominant flood generating mechanisms across the United States. *Geophysical Research Letters*, *43*, 4382–4390. https://doi.org/10.1002/2016GL068070

Blöschl, G., Hall, J., Parajka, J., Perdigão, R. A. P., Merz, B., Arheimer, B., et al. (2017). Changing climate shifts timing of European floods. *Science*, *357*(6351), 588–590. https://doi.org/10.1126/science.aan2506

Cai, X., Yang, Z.-L., Xia, Y., Huang, M., Wei, H., Leung, L. R., & Ek, M. B. (2014). Assessment of simulated water balance from Noah, Noah-MP, CLM, and VIC over CONUS using the NLDAS test bed. *Journal of Geophysical Research: Atmospheres*, *119*, 13,751–13,770. https://doi.org/10.1002/2014JD022113.Received

CSIWG. (2018). Paying it forward: The Path Toward Climate-Safe Infrastructure in California, Sacramento, CA. Report of the Climate-Safe Infrastructure Working Group to the California State Legislature and the Strategic Growth Council. Retrieved from http://resources.ca.gov/docs/climate/ab2800/AB2800_Climate-SafeInfrastructure_FinalWithAppendices.pdf

Das, T., Dettinger, M. D., Cayan, D. R., & Hidalgo, H. G. (2011). Potential increase in floods in California's Sierra Nevada under future climate projections. *Climatic Change*, *109*(Suppl 1), 71–94. https://doi.org/10.1007/s10584-011-0298-z

Das, T., Hidalgo, H. G., Pierce, D. W., Barnett, T. P., Dettinger, M. D., Cayan, D. R., et al. (2009). Structure and detectability of trends in hydrological measures over the Western United States. *Journal of Hydrometeorology*, *10*(4), 871–892. https://doi.org/10.1175/2009JHM1095.1

Dettinger, M. D., Cayan, D. R., Meyer, M. K., & Jeton, A. E. (2004). Simulated hydrologic responses to climate variations and change in the Merced, Carson, and American river basins, Sierra Nevada, California, 1900-2099. *Climatic Change*, *62*, 283–317. https://doi.org/https://doi.org/10.1023/B:CLIM.0000013683.13346.4f

Efron, B., & Tibshirani, R. (1986). Bootstrap methods for standard errors, confidence intervals, and other measures of statistical accuracy. *Statistical Science*, *1*(1), 54–77. https://doi.org/10.1214/ss/1177013815

Falcone, J. A., Carlisle, D. M., Wolock, D. M., & Meador, M. R. (2010). GAGES: A stream gage database for evaluating natural and altered flow conditions in the conterminous United States. *Ecology*, *91*(2), 621. https://doi.org/10.1890/09-0889.1

Fassnacht, S. R., & Records, R. M. (2015). Large snowmelt versus rainfall events in the mountains. *Journal of Geophysical Research: Atmospheres*, *120*, 2375–2381. https://doi.org/10.1002/2014JD022753

Feng, S., & Hu, Q. (2007). Changes in winter snowfall/precipitation ratio in the contiguous United States. *Journal of Geophysical Research*, *112*, D15109. https://doi.org/10.1029/2007JD008397

Ficklin, D. L., Abatzoglou, J. T., Robeson, S. M., Null, S. E., & Knouft, J. H. (2018). Natural and managed watersheds show similar responses to recent climate change. *Proceedings of the National Academy of Sciences*, *115*(34), 8553–8557. https://doi.org/10.1073/pnas.1801026115

Freudiger, D., Kohn, I., Stahl, K., & Weiler, M. (2014). Large-scale analysis of changing frequencies of rain-on-snow events with flood-generation potential. *Hydrology and Earth System Sciences*, *18*, 2695–2709. https://doi.org/10.5194/hess-18-2695-2014

Fritze, H., Stewart, I. T., & Pebesma, E. (2011). Shifts in Western North American snowmelt runoff regimes for the recent warm decades. *Journal of Hydrometeorology*, *12*(5), 989–1006. https://doi.org/10.1175/2011JHM1360.1

Gaure, S. (2013). lfe: Linear group fixed effects. *The R Journal*, *5*(2), 104–117. https://doi.org/10.32614/rj-2013-031

Gleick, P. H. (1987). Regional hydrologic consequences of increases in atmospheric CO2 and other trace gases. *Climatic Change*, *10*(2), 137–160. https://doi.org/10.1007/BF00140252

Gonzales, K. R., Swain, D. L., Nardi, K. M., Barnes, E. A., & Diffenbaugh, N. S. (2019). Recent warming of landfalling atmospheric rivers along the west coast of the United States. *Journal of Geophysical Research: Atmospheres*. https://doi.org/10.1029/2018JD029860

Hall, J., Arheimer, B., Borga, M., Brázdil, R., Claps, P., Kiss, A., et al. (2014). Understanding flood regime changes in Europe: A state-of-the-art assessment. *Hydrology and Earth System Sciences*, *18*(7), 2735–2772. https://doi.org/10.5194/hess-18-2735-2014

Hamlet, A. F., & Lettenmaier, D. P. (2007). Effects of 20th century warming and climate variability on flood risk in the western U.S. *Water Resources Research*, *43*, W06427. https://doi.org/10.1029/2006WR005099

Hamlet, A. F., Mote, P. W., Clark, M. P., & Lettenmaier, D. P. (2006). Twentieth-century trends in runoff, evapotranspiration, and soil moisture in the western United States. *Journal of Climate*, *20*, 1468–1486. https://doi.org/10.1175/JCLI4051.1

Harpold, A. A., Kaplan, M. L., Klos, P. Z., Link, T., McNamara, J. P., Rajagopal, S., et al. (2017). Rain or snow: Hydrologic processes, observations, prediction, and research needs. *Hydrology and Earth System Sciences*, *21*(1), 1–22. https://doi.org/10.5194/hess-21-1-2017

Harpold, A. A., & Kohler, M. (2017). Potential for changing extreme snowmelt and rainfall events in the mountains of the western United States. *Journal of Geophysical Research: Atmospheres*, *122*, 13,219–13,228. https://doi.org/10.1002/2017JD027704

Harr, R. D. (1981). Some characteristics and consequences of snowmelt during rainfall in western Oregon. *Journal of Hydrology*, *53*, 277–304. https://doi.org/10.1016/0022-1694(81)90006-8

Hirsch, R. M., & De Cicco, L. (2015). User guide to Exploration and Graphics for RivEr Trends (EGRET) and dataRetrieval: R packages for hydrologic data (version 2.0, February 2015). In *U.S. Geological Survey Techniques and Methods book 4, chap. A10* (p. 93 p.). https://doi.org/https://doi.org/10.3133/tm4A10

Hodgkins, G. A., Whitfield, P. H., Burn, D. H., Hannaford, J., Renard, B., Stahl, K., et al. (2017). Climate-driven variability in the occurrence of major floods across North America and Europe. *Journal of Hydrology*, *552*, 704–717. https://doi.org/10.1016/j.jhydrol.2017.07.027

Huang, X., Hall, A. D., & Berg, N. (2018). Anthropogenic warming impacts on today's Sierra Nevada Snowpack and flood risk. *Geophysical Research Letters*, *45*, 6215–6222. https://doi.org/10.1029/2018GL077432

Ivancic, T. J., & Shaw, S. B. (2015). Examining why trends in very heavy precipitation should not be mistaken for trends in very high river discharge. *Climatic Change*, *133*(4), 681–693. https://doi.org/10.1007/s10584-015-1476-1

Jeong, D. I., & Sushama, L. (2017). Rain-on-snow events over North America based on two Canadian regional climate models. *Climate Dynamics*, *50*(1-2), 303–316. https://doi.org/10.1007/s00382-017-3609-x

Kampf, S. K., & Lefsky, M. A. (2016). Transition of dominant peak flow source from snowmelt to rainfall along the Colorado Front Range: Historical patterns, trends, and lessons from the 2013 Colorado Front Range floods. *Water Resources Research*, *52*, 407–422. https://doi.org/10.1002/2015WR017784

Kattelmann, R. (1997). Flooding from rain-on-snow events in the Sierra Nevada. In G. H. Leavesley et al. (Eds.), *Destructive water: Water-Caused Natural Disasters, their Abatement and Control, Proceedings of the Conference Held at Anaheim, California, June 1996 (IAHS, pp. 59–65)*. Wallingford, UK: IASH Publication.

Klos, P. Z., Link, T. E., & Abatzoglou, J. T. (2014). Extent of the rain-snow transition zone in the western U.S. under historic and projected climate. *Geophysical Research Letters*, *41*, 2359–2367. https://doi.org/10.1002/2014GL059393

Knowles, N., Dettinger, M. D., & Cayan, D. R. (2006a). Trends in snowfall versus rainfall in the western United States. *Journal of Climate*, *19*, 4545–4559. https://doi.org/10.1175/JCLI3850.1

Li, D., Lettenmaier, D. P., Margulis, S. A., & Andreadis, K. (2019). The role of rain-on-snow in flooding over the conterminous United States. *Water Resources Research*. https://doi.org/10.1029/2019wr024950

Li, D., Wrzesien, M. L., Durand, M., Adam, J., & Lettenmaier, D. P. (2017). How much runoff originates as snow in the western United States, and how will that change in the future? *Geophysical Research Letters*, *44*, 6163–6172. https://doi.org/10.1002/2017GL073551

Lins, H. F., & Slack, R. (1999). Streamflow trends in the United States. *Geophysical Research Letters*, *26*(2), 227–230. https://doi.org/10.1029/1998GL900291

Loukas, A., Vasiliades, L., & Dalezios, N. R. (2002). Potential climate change impacts on flood producing mechanisms in southern British Columbia, Canada using the CGCMA1 simulation results. *Journal of Hydrology*, *259*, 163–188. https://doi.org/10.1016/S0022-1694(01)00580-7

Lundquist, J. D., Dettinger, M. D., & Cayan, D. R. (2005). Snow-fed streamflow timing at different basin scales: Case study of the Tuolumne River above Hetch Hetchy, Yosemite, California. *Water Resources Research*, *41*, W07005. https://doi.org/10.1029/2004WR003933

Mankin, J. S., & Diffenbaugh, N. S. (2015). Influence of temperature and precipitation variability on near-term snow trends. *Climate Dynamics*, *45*(3–4), 1099–1116. https://doi.org/10.1007/s00382-014-2357-4

Margulis, S. A., Cortés, G., Girotto, M., & Durand, M. (2016). A Landsat-Era Sierra Nevada Snow Reanalysis (1985–2015). *Journal of Hydrometeorology*, *17*(4), 1203–1221. https://doi.org/10.1175/JHM-D-15-0177.1

Martin, R. O. R., & Hanson, R. L. (1966). Reservoirs in the United States (Geological Survey Water-Supply Paper 1838). Retrieved from http://udspace.udel.edu/handle/19716/1589

McCabe, G. J., Clark, M. P., & Hay, L. E. (2007). Rain-on-snow events in the western United States. *Bulletin of the American Meteorological Society*, *2007*, 319–328. https://doi.org/10.1175/BAMS-88-3-3I9

McCabe, G. J., Wolock, D. M., & Valentin, M. (2018). Warming is driving decreases in snow fractions while runoff efficiency remains mostly unchanged in snow-covered areas of the western United States. *Journal of Hydrometeorology*, *19*(5), 803–814. https://doi.org/10.1175/JHM-D-17-0227.1

Merz, R., & Blöschl, G. (2003). A process typology of regional floods. *Water Resources Research*, *39*(12), 1340. https://doi.org/10.1029/2002WR001952

Milly, P. C. D., Betancourt, J., Falkenmark, M., Hirsch, R. M., Kundzewicz, Z. W., Lettenmaier, D. P., & Stouffer, R. J. (2008). Stationarity is dead: Whither Water Management? *Science*, *319*(5863), 573–574. https://doi.org/10.1126/science.1151915

Mitchell, K. E., Lohmann, D., Houser, P. R., Wood, E. F., Schaake, J. C., Robock, A., et al. (2004). The multi-institution North American Land Data Assimilation System (NLDAS): Utilizing multiple GCIP products and partners in a continental distributed hydrological modeling system. *Journal of Geophysical Research*, *109*, D07S90. https://doi.org/10.1029/2003jd003823

Mote, P. W. (2006). Climate-driven variability and trends in mountain snowpack in western North America. *Journal of Climate*, *19*(23), 6209–6220. https://doi.org/10.1175/JCLI3971.1

Mote, P. W., Li, S., Lettenmaier, D. P., Xiao, M., & Engel, R. (2018). Dramatic declines in snowpack in the western US. *Npj Climate and Atmospheric Science*, *1*(1), 1–6. https://doi.org/10.1038/s41612-018-0012-1

Musselman, K. N., Clark, M. P., Liu, C., Ikeda, K., & Rasmussen, R. (2017). Slower snowmelt in a warmer world. *Nature Climate Change*, *7*(3), 214–219. https://doi.org/10.1038/nclimate3225

Musselman, K. N., Lehner, F., Ikeda, K., Clark, M. P., Prein, A. F., Liu, C., et al. (2018). Projected increases and shifts in rain-on-snow flood risk over western North America. *Nature Climate Change*, *8*(9), 808–812. https://doi.org/10.1038/s41558-018-0236-4

Painter, T. H., Berisford, D. F., Boardman, J. W., Bormann, K. J., Deems, J. S., Gehrke, F., et al. (2016). The airborne snow observatory: Fusion of scanning lidar, imaging spectrometer, and physically-based modeling for mapping snow water equivalent and snow albedo. *Remote Sensing of Environment*, *184*, 139–152. https://doi.org/10.1016/j.rse.2016.06.018

Parajka, J., Kohnová, S., Bálint, G., Barbuc, M., Borga, M., Claps, P., et al. (2010). Seasonal characteristics of flood regimes across the Alpine-Carpathian range. *Journal of Hydrology*, *394*(1-2), 78–89. https://doi.org/10.1016/j.jhydrol.2010.05.015

Pitlick, J. (1994). Relation between peak flows, precipitation, and physiography for five mountainous regions in the western USA. *Journal of Hydrology*, *158*, 219–240. https://doi.org/10.1016/0022-1694(94)90055-8

Robinson, J. S., Sivapalan, M., & Snell, J. D. (1995). On the relative roles of hillslope processes, channel routing, and network geomorphology in the hydrologic response of natural catchments. *Water Resources Research*, *31*(12), 3089–3101. https://doi.org/10.1029/95WR01948

Rood, S. B., Foster, S. G., Hillman, E. J., Luek, A., & Zanewich, K. P. (2016). Flood moderation: Declining peak flows along some Rocky Mountain rivers and the underlying mechanism. *Journal of Hydrology*, *536*, 174–182. https://doi.org/10.1016/j.jhydrol.2016.02.043

Rosenberg, E. A., Wood, A. W., & Steinemann, A. C. (2011). Statistical applications of physically based hydrologic models to seasonal streamflow forecasts. *Water Resources Research*, *47*, W00H14. https://doi.org/10.1029/2010WR010101

Rupp, D. E., & Li, S. (2017). Less warming projected during heavy winter precipitation in the Cascades and Sierra Nevada. *International Journal of Climatology*, *37*(10), 3984–3990. https://doi.org/10.1002/joc.4963

Schlenker, W., & Roberts, M. J. (2009). Nonlinear temperature effects indicate severe damages to U.S. crop yields under climate change. *Proceedings of the National Academy of Sciences*, *106*(37), 15,594–15,598. https://doi.org/10.1073/pnas.0906865106

Sheffield, J., Pan, M., Wood, E. F., Mitchell, K. E., Houser, P. R., Schaake, J. C., et al. (2003). Snow process modeling in the North American Land Data Assimilation System (NLDAS): 1. Evaluation of model-simulated snow cover extent. *Journal of Geophysical Research*, *108*(D22), 8849. https://doi.org/10.1029/2002JD003274

Sivapalan, M., Jothityangkoon, C., & Menabde, M. (2002). Linearity and nonlinearity of basin response as a function of scale: Discussion of alternative definitions. *Water Resources Research*, *38*(2), 1012. https://doi.org/10.1029/2001WR000482

Slater, L. J., & Villarini, G. (2016). Recent trends in U.S. flood risk. *Geophysical Research Letters*, *43*, 12,428–12,436. https://doi.org/10.1002/2016GL071199

Solander, K. C., Bennett, K. E., & Middleton, R. S. (2017). Shifts in historical streamflow extremes in the Colorado River Basin. *Journal of Hydrology: Regional Studies*, *12*, 363–377. https://doi.org/10.1016/j.ejrh.2017.05.004

Steinschneider, S., Yang, Y.-C. E., & Brown, C. (2013). Panel regression techniques for identifying impacts of anthropogenic landscape change on hydrologic response. *Water Resources Research*, *49*, 7874–7886. https://doi.org/10.1002/2013WR013818

Stewart, I. T. (2009). Changes in snowpack and snowmelt runoff for key mountain regions. *Hydrological Processes*, *23*(1), 78–94. https://doi.org/10.1002/hyp

Stewart, I. T., Cayan, D. R., & Dettinger, M. D. (2005). Changes toward earlier streamflow timing across western. *Journal of Climate*, *18*, 1136–1155. https://doi.org/10.1007/978-3-642-10248-6_1

Sui, J., & Koehler, G. (2001). Rain-on-snow induced flood events in southern Germany. *Journal of Hydrology*, *252*, 205–220. https://doi.org/10.1016/S0022-1694(01)00460-7

Surfleet, C. G., & Tullos, D. (2013). Variability in effect of climate change on rain-on-snow peak flow events in a temperate climate. *Journal of Hydrology*, *479*, 24–34. https://doi.org/10.1016/j.jhydrol.2012.11.021

Tavares, T., & Kracher, G. (2017). Winter storms exact historic roads toll. The Mile Marker: A Caltrans Performance Report. Retrieved from http://www.dot.ca.gov/milemarker/docs/articles/2017/Q2/MM-2017-Q2-winter.pdf

Tohver, I. M., Hamlet, A. F., & Lee, S.-Y. (2014). Impacts of 21st-century climate change on hydrologic extremes in the Pacific Northwest Region of North America. *Journal of the American Water Resources Association*, *50*(6), 1461–1476. https://doi.org/10.1111/jawr.12199

Toms, J. D., & Lesperance, M. L. (2003). Piecewise regression: A tool for identifying ecological thresholds. *Ecology*, *84*(8), 2034–2041. https://doi.org/10.1890/0012

Vivoni, E. R., Di Benedetto, F., Grimaldi, S., & Eltahir, E. A. B. (2008). Hypsometric control on surface and subsurface runoff. *Water Resources Research*, *44*, W12502. https://doi.org/10.1029/2008WR006931

Vivoni, E. R., Entekhabi, D., Bras, R. L., & Ivanov, V. Y. (2007). Controls on runoff generation and scale-dependence in a distributed hydrologic model. *Hydrology and Earth System Sciences*, *11*, 1683–1701. https://doi.org/10.5194/hess-11-1683-2007

Vormoor, K., Lawrence, D., Schlichting, L., Wilson, D., & Wong, W. K. (2016). Evidence for changes in the magnitude and frequency of observed rainfall vs. snowmelt driven floods in Norway. *Journal of Hydrology*, *538*, 33–48. https://doi.org/10.1016/j.jhydrol.2016.03.066

Wilby, R. L. (2006). When and where might climate change be detectable in UK river flows? *Geophysical Research Letters*, *33*, L19407. https://doi.org/10.1029/2006GL027552

Wright, S. P. (1992). Adjusted p-values for simultaneous inference. *Biometrics*, *48*(4), 1005–1013. https://doi.org/10.1016/j.ecolmodel.2004.04.024

Xia, Y., Mitchell, K., Ek, M., Cosgrove, B., Sheffield, J., Luo, L., et al. (2012). Continental-scale water and energy flux analysis and validation for North American Land Data Assimilation System project phase 2 (NLDAS-2): 2. Validation of model-simulated streamflow. *Journal of Geophysical Research*, *117*, D03110. https://doi.org/10.1029/2011JD016051

Xia, Y., Mitchell, K., Ek, M., Sheffield, J., Cosgrove, B., Wood, E., et al. (2012). Continental-scale water and energy flux analysis and validation for the North American Land Data Assimilation System project phase 2 (NLDAS-2): 1. Intercomparison and application of model products. *Journal of Geophysical Research*, *117*, D03109. https://doi.org/10.1029/2011JD016048

Yan, H., Sun, N., Wigmosta, M., Skaggs, R., Hou, Z., & Leung, R. (2018). Next-generation intensity-duration-frequency curves for hydrologic design in snow-dominated environments. *Water Resources Research*, *54*, 1093–1108. https://doi.org/10.1002/2017WR021290

Yan, H., Sun, N., Wigmosta, M., Skaggs, R., Leung, L. R., Coleman, A., & Hou, Z. (2019). Observed spatiotemporal changes in the mechanisms of extreme water available for runoff in the Western United States. *Geophysical Research Letters*, *46*, 767–775. https://doi.org/10.1029/2018GL080260

Ziegler, A. D., Maurer, E. P., Sheffield, J., Nijssen, B., Wood, E. F., & Lettenmaier, D. P. (2005). Detection time for plausible changes in annual precipitation, evapotranspiration, and streamflow in three Mississippi River sub-basins. *Climatic Change*, *72*(1-2), 17–36. https://doi.org/10.1007/s10584-005-5379-4